Theoretical and Numerical Analysis of Applicability of Elliptical Cross-Section on Energy Dissipation of Hydraulic Jump

Rasoul Daneshfaraz[1,*], Hamidreza Abbaszadeh[2], Ehsan Aminvash[3]

[1]Department of Civil Engineering, Faculty of Engineering, University of Maragheh, Maragheh, Iran

[2]Department of Civil Engineering, Faculty of Engineering, University of Maragheh, Maragheh, Iran

[3]Department of Civil Engineering, Faculty of Engineering, University of Maragheh, Maragheh, Iran

*Correspondence e-mail: daneshfaraz@maragheh.ac.ir

Abstract

The destructive energy of water destroys hydraulic structures and reduces their effectiveness. In the present study, the effect of elliptical-shaped contraction has been investigated to reduce flow energy using FLOW-3D software. In the present study, the values of contraction are 10 and 15 cm. The results showed that the statistical indexes in the RNG turbulence model such as percentage Relative Error (RE%), Absolute Error (AE), Root Mean Square Error (RMSE) and Kling Gupta Efficiency (KGE) yield acceptable accuracy results compared to other turbulence models such as the k-ε, k-ω, and LES. In this study, the amplitude of the Froude number as the most effective dimensionless parameter in energy dissipation varied from 2.8 to 7.5. The results showed that in 10 cm elliptical-shaped contractions, the ratio of energy dissipation to the upstream and downstream specific energy was 24.62% and 29.84%, more than the classical hydraulic free jump, respectively. For the contractions of 15 cm, these values were 46.14% and 48.42%, respectively. In addition, by examining the obtained results, it was observed that the elliptical-shaped contractions have a better performance in terms of energy dissipation compared to the sudden contraction, obtained from the previous studies. By increasing the upstream Froude number, the relative energy dissipation increased so that the application of contraction reduces the downstream Froude number of the contracted cross-section in the range of 1.6 to 2.3. In this study, based on dimensional analysis, non-linear polynomial regression equations were presented to predict the relative energy dissipation ($\Delta E_{AB}/E_A$, $\Delta E_{AB}/E_B$).

Keywords: Elliptical-shaped contraction; Energy dissipation; Free hydraulic jump; Submerged hydraulic jump; FLOW-3D

1. INTRODUCTION

One of the most significant problems that exist downstream of hydraulic structures is the high kinetic energy of the flow, which must be consumed by the controlling structures. In case of lack of control, downstream structures may be destroyed and significant damages may be caused. Energy dissipator structures are installed downstream of hydraulic structures to control water, reduce the flow velocity and consume the energy of the flow. The energy dissipation is directly related to the turbulence of the flow, that's why a significant amount of energy dissipation can be achieved by shrinking an area of the channel. Creating a contraction in the flow path by creating a hydraulic jump when the flow collides with the contraction elements consumes part of the destructive kinetic energy and some of this energy is taken with the help of obstacles. Energy dissipation by different types of structures and methods, such as changing the geometric characteristics of the bed, including creating roughness, changing the shape of the section, using a stilling basin, using grid plates in the flow path, using divergent and convergent transformations and its effect on the characteristics of hydraulic jump has been the focus of researchers. The reduction of the channel width or the sudden contraction of the cross-sectional area in the flow path may be caused by the construction of structures such as bridge foundations, which will also block the passing flow. Yarnell [1] has done extensive laboratory studies on the contraction of bridge piers and theoretical analysis to limit the contraction coefficient. The investigations conducted by him showed that the depth of the flow retreat before the bridge foundations depends on the shape of the nose and the length of the bridge foundations. In addition, Chow [2] and Henderson [3] conducted studies in the field of flow blockage. Chow [2] mentioned the types of obstructions in the flow path including bridge piers, piers, and spillway supports. The results of Henderson [3] showed that placing the foundations at the same angle with the flow (the angle is less than 10 degrees) has a negligible effect on the flow retardation. Hager and Dupraz [4] investigated the characteristics of flow in discontinuous contraction in a laboratory manner. They reported a good correlation between their research results and theoretical relationships. Wu and Molinas [5] investigated the subcritical flow in the face of a short contraction during the flow. The relationship presented by them for calculating the flow rate has shown a suitable overlap with the results of previous research. Dey and Raikar [6] investigated scouring in long contraction.

Their results showed that the scour depth increases with the reduction of the contracted width. Jan and Chang [7] also investigated the hydraulic jump on a contracted shoot. Based on the experimental results, they concluded that the value of the relative hydraulic jump length significantly depends on the angle of the bed and is independent of the angle of contraction of the side walls. In addition, they presented theoretical relations for the sequent depth of the jump by considering the contracted cross-section and the slope of the floor. Das *et al.* [8] conducted studies related to energy dissipation in contracted shoots. Their results showed that the energy dissipation increases with the increase in the slope of the shoots. Sadeghfam *et al.* [9] investigated the behavior of screens in the supercritical flow in the Froude number range of 2.5 to 8.5 and reported more energy dissipation in screens compared to free hydraulic jump even in submerged jump conditions. Babaali *et al.* [10] evaluated the hydraulic jump in the stilling basin with converging walls using FLOW-3D software. The results showed that the energy dissipation in the stilling basin with a converging wall is much higher than in the stilling basin with its parallel form. In addition, they declared the best degree of convergence for energy dissipation to be 5 degrees. Habibzadeh *et al.* [11] investigated the characteristics of the hydraulic jump after the gate. They reported an increase in water level fluctuations with an increase in Froude number. Ghaderi *et al.* [12] numerically investigated free and submerged hydraulic jumps on different shapes of roughness in various roughness arrangements and different Froude number conditions in vertical sluice gates. Their results showed that the numerical model is well able to simulate the characteristics of the free and submerged jump. Ghaderi *et al.* [13] using FLOW-3D investigated the effect of triangular roughness on jump characteristics, including longitudinal characteristics of streamlines, flow patterns in the cavity area, horizontal velocity profiles and velocity distribution in the direction of flow.

Among the existing cases of contractions in nature, we can mention the existence of bridge foundations inside the river or channels. According to the investigations carried out so far, no study has been done regarding the use of elliptical-shaped contraction to dissipate the flow energy in a wide range of Froude numbers, and the report of the results of this type of structure is empty among scientific sources. Therefore, according to the importance of the subject, in the current research, the need to investigate the effect of elliptical-shaped contractions sections has been done in the

supercritical flow condition in terms of energy dissipation. In this research, the energy dissipation has been investigated in the elliptical-shaped contraction in the range of 2.8 to 7.5 of the Froude number. In addition, the results compared with the previous studies.

2. MATERIALS AND METHODS

### 2.1. Types of Hydraulic Jump in the Contraction under Supercritical Flow

By placing contraction, three types of hydraulic jump behavior can be observed. If the hydraulic jump occurs before the contraction, and the contraction is located in the subcritical region, the first type of behavior occurs (Figure 1a). If the distance between the starting point of the hydraulic jump and the contraction is not enough for the free hydraulic jump to occur, the behavior of the second type will be visible (Figure 1b). This type is an imposed hydraulic jump and the contraction is placed in the supercritical region. Due to the disturbances created, the energy dissipation in the behavior of the second type is more than the behavior of the first type. In addition, according to Figure 1(c), as a result of the collision of the supercritical flow with the contraction, the behavior of the third type occurs, which is called submerged hydraulic jump.
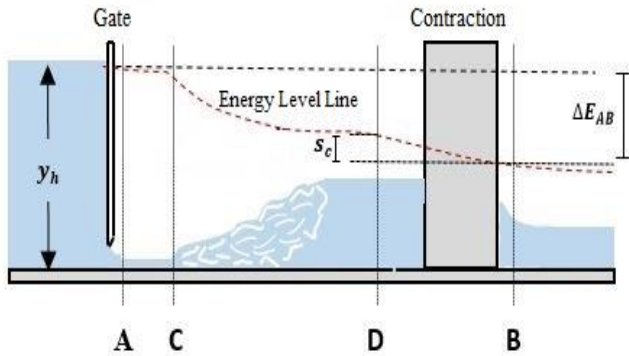
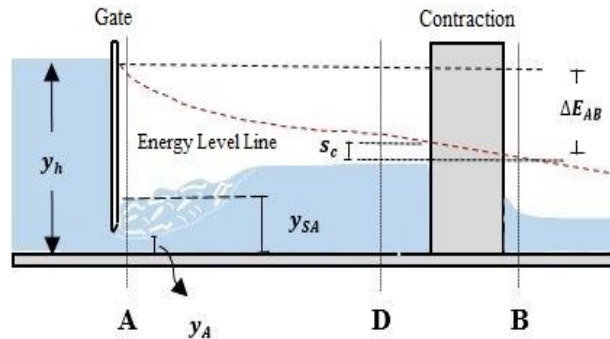(a)   (b)
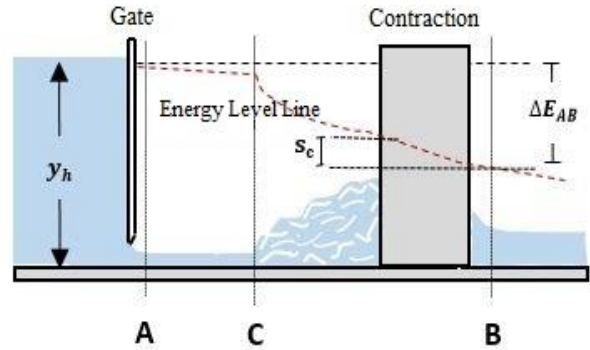
(c)

Fig. 1. Schematic diagram of flow with contraction (a) first type behavior (b) second type behavior (c) third type behavior

2.2. Calculation of Energy Dissipation

Using the principle of energy, the amount of energy dissipation between sections A and B is calculated according to Equ. (1) for types 1 and 2.

$$\Delta E_{AB} = E_A - E_B = (y_A + \frac{V_A^2}{2g}) - (y_B + \frac{V_B^2}{2g}) \tag{1}$$

In Equ. (1), y_A and y_B are the flow depth (L), V_A and V_B are the flow velocity in sections A and B (LT^{-1}), respectively, g is the gravitational acceleration (LT^{-2}) E_A is the specific energy of water in section A (L) and E_B is the specific energy of water in section B (L). The calculation of velocity in sections A and B is obtained by calculating the averaged velocity in the experiments. The flow depth in section A is calculated using Equ. (2) and in section B by measurement.

$$y_A = C_c \times d \tag{2}$$

In Equ. (2), d is the gate opening (L) and C_C is the flow contraction coefficient (-), which is calculated from the analytical results of Belaud *et al.* [14] based on the ratio of the gate opening to the upstream water depth for free and submerged flows.

For the third type, the energy dissipation, which includes energy dissipation due to submerged jump, energy dissipation due to contraction, and eddy flows before contraction, is calculated according to Equ. (4). The difference between the third type and the other types is how to calculate the flow velocity and depth in section A. So, the eddy flow created in section A makes it difficult to measure the depth. The submerged depth (y_{SA} (L)) is obtained using the water depth behind the gate as in Equ. (3).

$$y_{SA} = y_h - \frac{V_A^2}{2g} \tag{3}$$

2.4. Statistical Indexes

Here, statistical indicators of percentage relative error (RE%), root mean square error (RMSE) and Kling Gupta efficiency (KGE) have been used to predict the capability and accuracy of the proposed equation in estimating

$$\Delta E_{AB} = (y_{SA} + \frac{V_A^2}{2g}) - (y_B + \frac{V_B^2}{2g}) \tag{4}$$

In Equ. (3), the value of V_A can be calculated based on y_A obtained through Equ. (2).

2.3. Dimensional Analysis

The parameters affecting flow energy dissipation are:

$$f_1(Q, W, B, l, d, X, E_A, E_B, y_A, y_B, g, \rho, \mu) = 0 \tag{5}$$

where Q is the discharge (L^{3}T^{-1}), W is the channel width (L), B is the contraction (L), l is the contraction length (L), X is the distance between the contraction and the gate (L),

ρ is the water density (ML^{-3}) and μ is the dynamic viscosity (ML^{-1}T^{-1}). Using the π-Buckingham, the dimensionless parameters can be rewritten according to Equ. (6).

$$f_2(\frac{Q}{g^{0.5} y_A^{2.5}}, \frac{W}{y_A}, \frac{B}{y_A}, \frac{l}{y_A}, \frac{d}{y_A}, \frac{X}{y_A}, \frac{E_A}{y_A}, \frac{E_B}{y_A}, \frac{y_B}{y_A}, \text{Re}) = 0 \tag{6}$$

Some of the parameters of Equ. (6) have certain values, such as l, d, and X, so the influence of these parameters can be omitted. Since the flow is turbulent and 46238≥ Re≥17807, therefore, the effect of the Reynolds number (-) can be ignored (Daneshfaraz *et al.* [15]). In addition, to make the parameters meaningful by dividing parameters $\frac{B}{y_A}$ and $\frac{W}{y_A}$ by each other, the dimensional analysis of the present research is presented as Equ. (7):

$$\frac{\Delta E_{AB}}{E_A}, \frac{\Delta E_{AB}}{E_B} = f_3(Fr_A, \frac{B}{W}, \frac{y_B}{y_A}) \tag{7}$$

In Equ. (7) Fr_A represents the Froude number (-).

relative energy dissipation. Statistical criteria for estimating the relative energy dissipation were calculated from Equs (8), (9) and (10), respectively.

$$RE\% = \left|\frac{X_{Obs} - X_{Cal}}{X_{Obs}}\right| \times 100 \tag{8}$$

$$RMSE = \sqrt{\frac{\sum_{i=1}^{n}(X_{Obs} - X_{Cal})_i^2}{n}} \tag{9}$$

$$KGE = 1 - \sqrt{(R-1)^2 + (\beta-1)^2 + (\gamma-1)^2}$$

$$\beta = \frac{\overline{X_{cal}}}{\overline{X_{obs}}}, \gamma = \frac{\sigma_{Cal}/\overline{X_{cal}}}{\sigma_{cal}/\overline{X_{obs}}}$$

$$\begin{aligned} 0.7 &< KGE < 1 \quad very\ good \\ 0.6 &< KGE < 0.7 \quad good \\ 0.5 &< KGE \leq 0.6 \quad satisfactory \\ 0.4 &< KGE \leq 0.5 \quad acceptable \\ KGE &\leq 0.4 \quad unsatisfactory \end{aligned} \tag{10}$$

$$R = \frac{[\sum_{i=1}^{n}(X_{Obs\ i} - \overline{X_{Obs}}) \times (X_{Cal\ i} - \overline{X_{Cal}})]}{\sum_{i=1}^{n}(X_{Obs\ i} - \overline{X_{Obs}})\sum_{i=1}^{n}(X_{Cal\ i} - \overline{X_{Cal}})}$$

2.5. Flow Governing Equations

The continuity and Navier-Stokes equations are discretized by FLOW-3D software to perform three-dimensional simulation of fluid motion. The continuity equation in a fluid stream is as follows (Flow Science Inc., [16]).

where u_i is the velocity component of the direction i. FLOW-3D software solves the Navier-Stokes equations for three-dimensional flow analysis using the VOF on a networked field. The equations in the Cartesian coordinate system are obtained by the following equations (Daneshfaraz *et al.* [17]).

$$\frac{\partial \rho}{\partial t} + \frac{\partial}{\partial x_i}(\rho u_i) = 0 \tag{11}$$

$$V_F \frac{\partial \rho}{\partial t} + \frac{\partial}{\partial x}(\rho u A_x) + R\frac{\partial}{\partial y}(\rho v A_y) + \frac{\partial}{\partial z}(\rho w A_z) = R_{SOR} + R_{DIF} \tag{12}$$

$$\frac{\partial u}{\partial t} + \frac{1}{V_F}\left(u A_x \frac{\partial u}{\partial x} + v A_y \frac{\partial u}{\partial y} + w A_z \frac{\partial u}{\partial z}\right) = -\frac{1}{\rho}\frac{\partial P}{\partial x} + G_x + f_x \tag{13}$$

$$\frac{\partial v}{\partial t} + \frac{1}{V_F}\left(u A_x \frac{\partial v}{\partial x} + v A_y \frac{\partial v}{\partial y} + w A_z \frac{\partial v}{\partial z}\right) = -\frac{1}{\rho}\frac{\partial P}{\partial y} + G_y + f_y \tag{14}$$

$$\frac{\partial w}{\partial t} + \frac{1}{V_F}\left(u A_x \frac{\partial w}{\partial x} + v A_y \frac{\partial w}{\partial y} + w A_z \frac{\partial w}{\partial z}\right) = -\frac{1}{\rho}\frac{\partial P}{\partial z} + G_z + f_z \tag{15}$$

In the above equations, *u, v* and *w* are velocity components, A_x, A_y and A_z are a fraction of the area associated with the flow, G_x, G_y and G_z are the body acceleration, f_x, f_y, and f_z are the viscosity acceleration in the directions of *x, y* and *z*,

R_{SOR} is the mass source, R_{DIF} is the expression of turbulence, V_F is the fluid volume fraction, and *P* is the pressure. This equation is generally expressed as Equ. (16).

$$\rho\left(\frac{\partial u_i}{\partial t} + u_j\frac{\partial u_i}{\partial x_i}\right) = -\frac{\partial P}{\partial x_i} + B_i + \frac{\partial}{\partial x_j}\left[\mu\left(\frac{\partial u_i}{\partial x_j} + \frac{\partial u_j}{\partial x_i} - \frac{2}{3}\delta_{ij}\frac{\partial u_k}{\partial x_k}\right)\right] \tag{16}$$

where B_i is the volumetric force in direction i and μ is the dynamic viscosity of the fluid, ρ is the water density, x_i, x_j and x_k are the flow coordinates in the spatial direction i, j and k, respectively. δ_{ij} is Kronecker delta, where, if $i=j$ its value is equal to 1 otherwise, it has a zero value (Daneshfaraz *et al.* [18]).

2.6. Definition of the Solution Network and Boundary Conditions

In this research, the energy dissipation in elliptical-shaped contractions was investigated using FLOW-3D software under free and submerged flow conditions. Validation was done using the laboratory data of Daneshfaraz *et al.* [19], then the models were implemented for different hydraulic conditions. Figure 2 shows the three-dimensional geometry of the model. In addition, Table 1 shows the hydraulic and geometric characteristics of the model in this research.
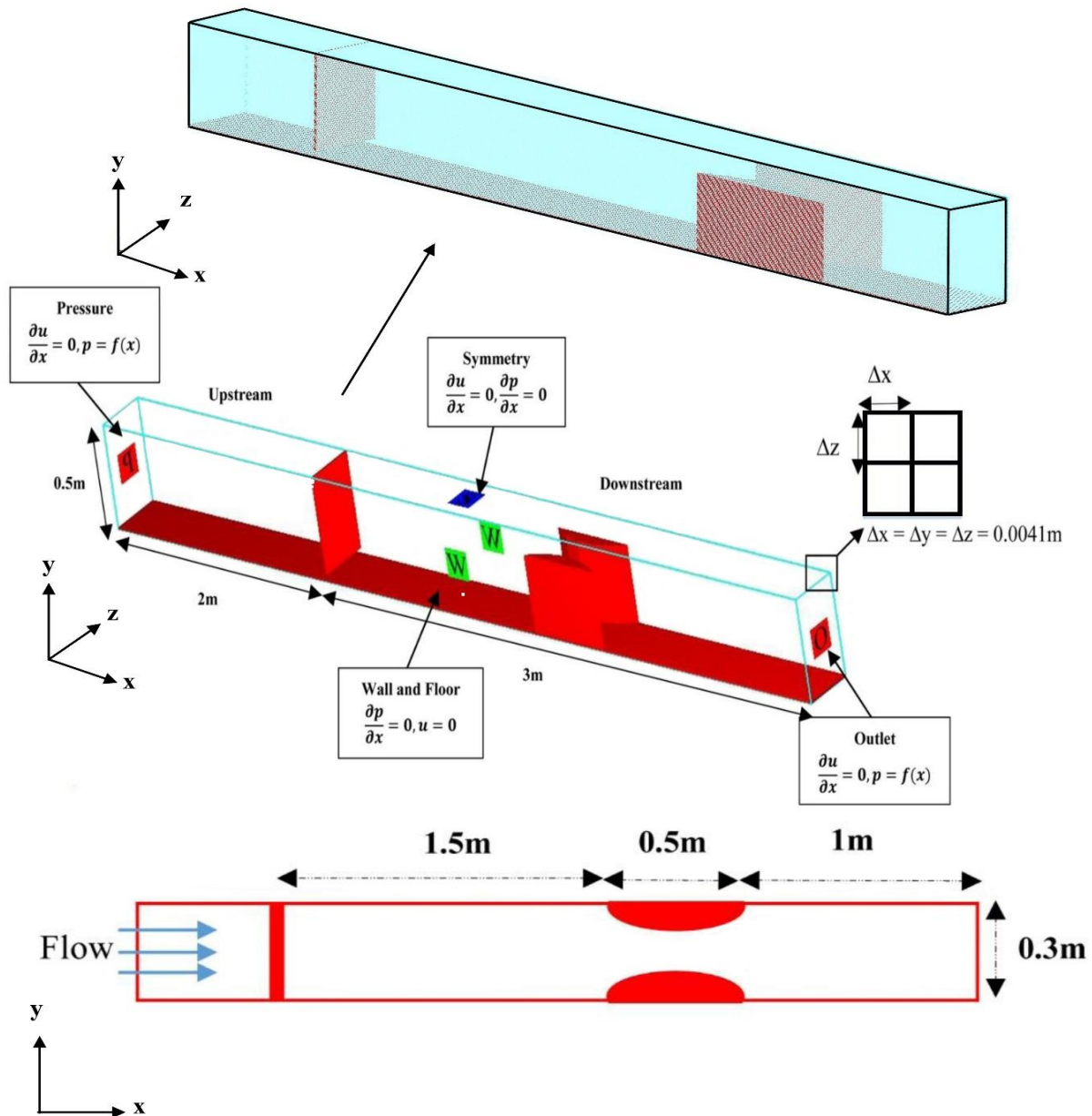

Fig.2. 3-D geometry of models

Daneshfaraz, R.,, Abbaszadeh, H., Aminvash, E.,ORCID: 0000-0003-1012-8342, ORCID: 0000-0001-7714-6081, ORCID: 0000-0001-8901-2232, Turkish

Table 1. Hydraulic and geometric characteristics of the model

Upstream flow depth (cm)	Froude number (-)	Reynolds number (-)	Geometry dimensions of the model (cm)	Gate opening (cm)	The total amount of contraction from the sides (cm)
9.7-28.3	2.8-7.5	17807-46238	300×30×32	2.6	10-15

In this research, the optimal mesh was selected by performing simulation in 4 modes with different mesh dimensions (Table 2).

Table 2. Experimental and numerical results with different mesh dimensions

Mode	Mesh dimensions (cm)	$\Delta E_{AB}/E_A$ (-) experimental	$\Delta E_{AB}/E_A$ (-) numerical	RE (%)	AE (-)	RMSE (-)	KGE (-)
1	0.6	0.510	0.448	12.176	0.062	0.0718	good
2	0.5	0.510	0.521	2.112	0.011	0.0376	Very good
3	0.41	0.510	0.513	0.534	0.003	0.0108	Very good
4	0.38	0.510	0.512	0.374	0.002	0.0106	Very good

By comparing the errors obtained in modes 1, 2, 3, and 4, it can be seen that the RE%, AE, and RMSE in mode No.4 are lower than in other modes. Since the error obtained in modes, 3 and 4 is very close to each other; therefore the third case is considered the optimal mesh with the 4168008 meshes. For this mode, the RE%, AE, and RMSE are 0.534, 0.003, and 0.0108, respectively.

In this study, the fluid range behind the gate was defined as the initial condition for the simulation. In addition, the pressure distribution was defined hydrostatically. Table 3 shows the boundary conditions in the current research.

Table 3. Boundary conditions of models

Inlet boundary condition	Outlet boundary condition	upper boundary condition	floor and walls Boundary condition
Pressure (P)	Out (O)	Symmetry (S)	Wall (W)

2.7. Turbulence Models

In this research, to choose the turbulence model, simulations were performed on RNG, k-ε, k-ω, and LES models, and the RNG model was chosen to continue the simulations. Among the reasons for choosing this model, we can mention reliability in answering various problems, accurate solution of equations, high accuracy in showing

details of the flow and review of previous studies (Ghaderi *et al*. [12]; Daneshfaraz *et al*. [17]). On the other hand, according to Table 4, the comparison of the simulation

results of the turbulence models shows that the RE%, AE, and RMSE have the lowest value.

Table 4. Turbulence models

Turbulence model	$\Delta E_{AB}/E_A$ (-) experimental	$\Delta E_{AB}/E_A$ (-) numerical	RE (%)	AE (-)	RMSE (-)	KGE (-)
RNG	0.510	0.513	0.534	0.003	0.0108	Very good
k-ε	0.510	0.516	1.229	0.006	0.0148	Very good
k-ω	0.510	0.518	1.574	0.008	0.0235	Very good
LES	0.510	0.521	2.207	0.011	0.0255	Very good

3. RESULTS AND DISCUSSION

For validation, the simulation results were plotted with the experimental results of Daneshfaraz *et al*. [19] (Figure 3).

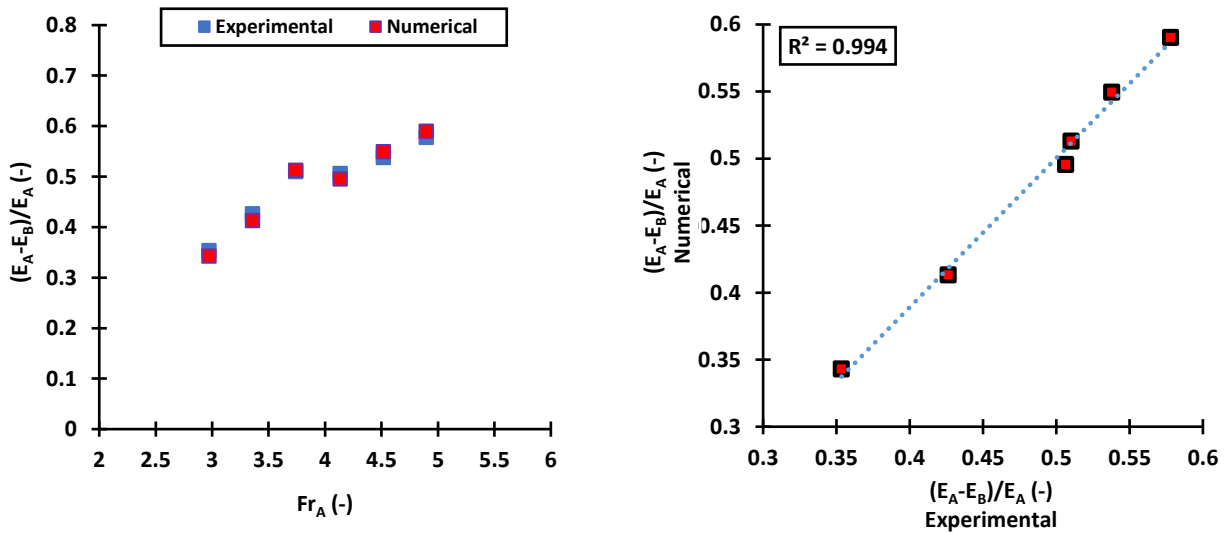The numerical solution results are the same as the experimental results and the determination coefficient is 0.994.

Fig. 3. Fitting and comparing the relative energy dissipation obtained from experimental results and numerical solution

Figure 4(a-b) shows the surface profile of the flow passing through the gate, or in other words, shows the formation of a free and submerged hydraulic jump for contractions of 10 and 15 cm at a depth of 17.7 cm behind the gate. Also,

Figure 4(c,d) shows the longitudinal profile of the depth averaged velocity in the X-Z section and Figure 4(e,f) represents the longitudinal profile of the depth averaged velocity in the X-Y section. In the narrowing of 15 cm, due

to the formation of a submerged hydraulic jump and increasing in the flow depth after the gate, the depth averaged velocity has decreased. Also, by reducing the flow depth after the contraction, the depth averaged velocity has increased.
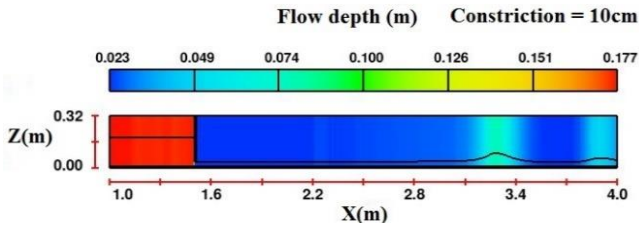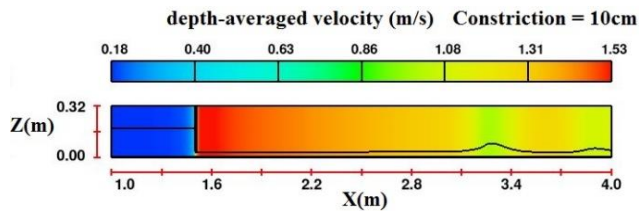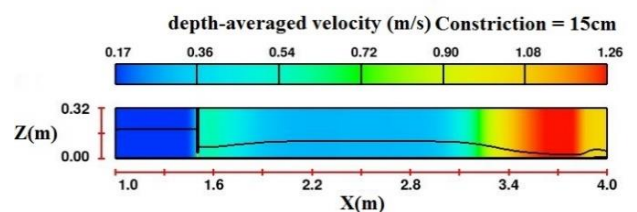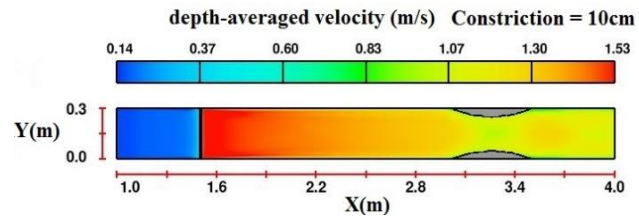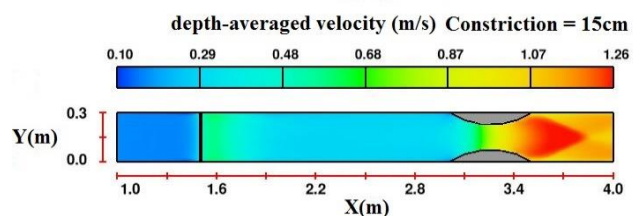

(a)
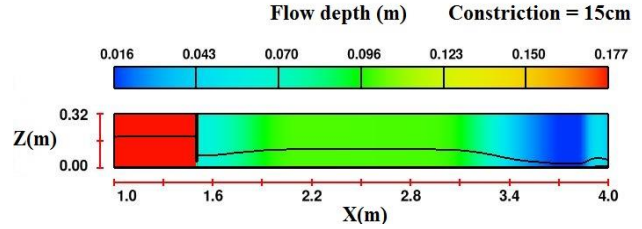
(b)

(c)

(d)

(e)

(f)

Fig. 4. Longitudinal profiles of flow and depth averaged velocity obtained from FLOW-3D software, (a,b) Longitudinal profile, (c,d) Velocity profile of transverse section, (e,f) Velocity profile of plan section

In Figure 5, the horizontal axis is the Froude number in section A (Fr_A) and the vertical axis indicates the ratio of energy dissipation between sections A and B to the specific energy in sections A and B ($\Delta E_{AB}/E_A$, $\Delta E_{AB}/E_B$). The energy dissipation due to the elliptical contraction is more than the classical free hydraulic jump, which can be justified by the presence of turbulent flows in the area before the contraction. In the free hydraulic jump, the energy dissipation is only caused by the hydraulic jump, while according to the energy level line, in the elliptical contraction, in addition to the energy dissipation caused by the hydraulic jump, there is also a local loss and a loss caused by the contraction elements. Also, the phenomenon of flow recoil has a significant effect on energy dissipation, so that the flow recoil increases the depth in the contraction area, so the energy dissipation will be increased.
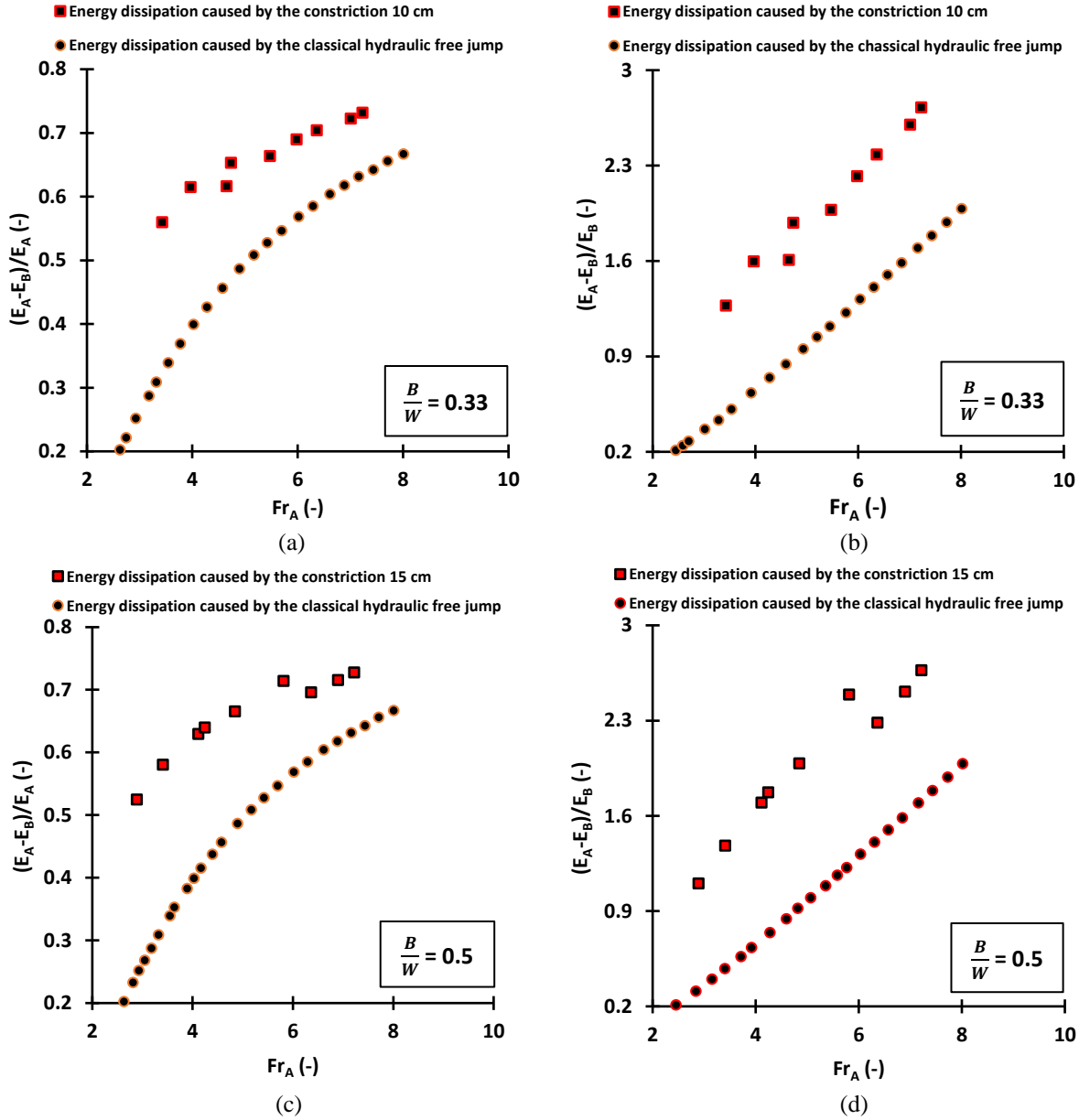
Fig. 5. Changes in energy dissipation relative to (a,c) upstream in the 10 and 15 cm contraction (b,d) downstream in the 10 and 15 cm contraction in the range of different Froude number

In the simulation, the upstream depth is entered the same for the contractions of 10 and 15 cm in models. Therefore, the discharge entering the flume in the mentioned contractions will be different from each other, so that the inlet discharge to supply the expected water in the contraction of 10 cm will be more than the contraction of 15 cm. For example, for an upstream water depth of 9.7 cm, the discharge for contractions of 10 and 15 cm is 5.34 and 6.34 L/s, respectively, which can be attributed to the greater opening of the cross-section in the 10 cm contraction, which allows more water to pass through it. With the investigations carried out from Figure 5, it was observed that with the increase of the Froude number in each of the models, the energy dissipation increases. The reason for this can be pointed to the low depth of the water after the gate and consequently the high velocity of the passing flow,

in which the hydraulic jump is accompanied by more turbulence and interference with the air, which itself causes an increase in the tailwater depth. In addition, the phenomenon of flow recoil has a significant effect on energy dissipation, which increases the depth in the contraction area, so the energy dissipation increases. A comparison was made between the results of the current research and the results of previous studies (Figure 6). It should be noted that no study has been done regarding the use of elliptical elements for energy consumption, but in this regard, we can refer to the research of Daneshfaraz *et al.* [19] on the use of sudden contraction. The similarity of

the present study with the research of Daneshfaraz *et al.* [19] is in the size of the contraction and their difference is in the type of contraction. In Figure 6(a-b), it was observed that the relative energy dissipation in elliptical-shaped contraction is higher than the sudden contraction in 10 cm narrowing. In addition, according to Figure 6(c-d), the relative energy dissipation in the 15 cm elliptical-shaped contraction is more than the sudden contraction of 15 cm. So in all cases of the model, the elliptical contraction leads to more energy dissipation compared to a sudden contraction.
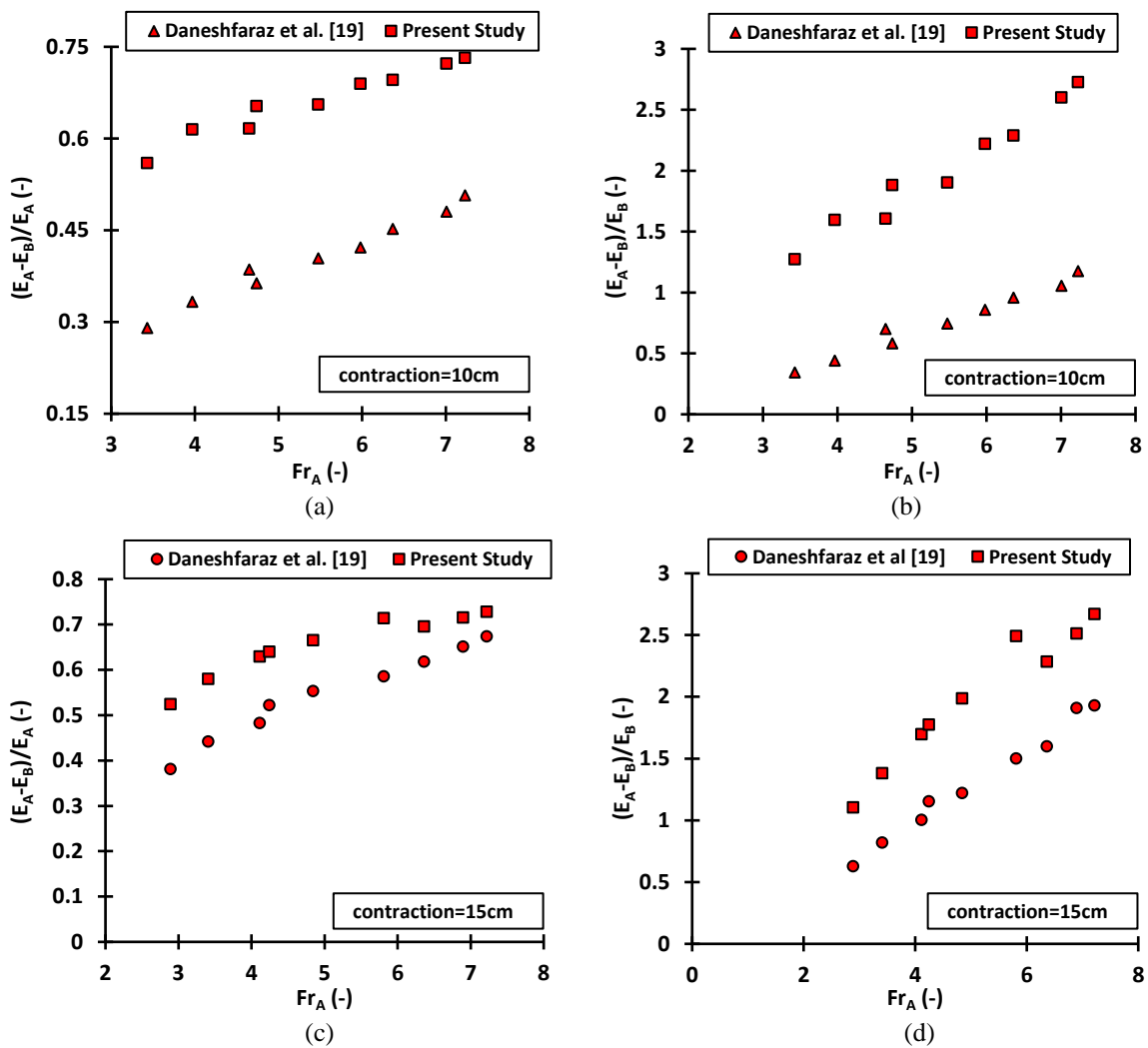
Fig. 6. Comparing the results of relative energy dissipation of the present study with the previous study

Daneshfaraz, R.,, Abbaszadeh, H., Aminvash, E.,ORCID: 0000-0003-1012-8342, ORCID: 0000-0001-7714-6081, ORCID: 0000-0001-8901-2232, Turkish Journal of Hydraulics: Theoretical and Numerical Analysis of Applicability of Elliptical Cross-Section on Energy Dissipation of Hydraulic Jump,Vol :6 , Number : 2, Page : 22-35 (2022)

The results showed that the use of the elliptical-shaped contraction has a great effect on energy dissipation. So that the Froude number downstream of the channel is reduced from 2.8-7.5 to 1.6-2.3. The performance of hydraulic structures in terms of energy dissipation can affect the stability and resistance of the construction in the rivers and channels. In the design of depreciating structures, the efficiency of the structure should be investigated. In the construction of USBR stilling basins, each stilling basin is built according to its own Froude number; therefore, there is a limitation of Froude number for the design of USBR stilling basins. So that the minimum Froude number for using USBR II and USBR III is 4.5, and for $Fr < 4$, special attachments must be considered. In addition, the USBR IV is used to control the hydraulic jump, when $4.5 < Fr < 2.5$. In addition, in stilling basins, sufficient time and cost, special components and materials, skilled labor and high precision in design and construction are needed, while the design and construction of crescent-shaped contraction are affordable. For the Froude number range of 2.8 to 5.7, a type 3 stilling basin should be used, but the results show that elliptical-shaped contraction can be an alternative for this type of stilling basin.
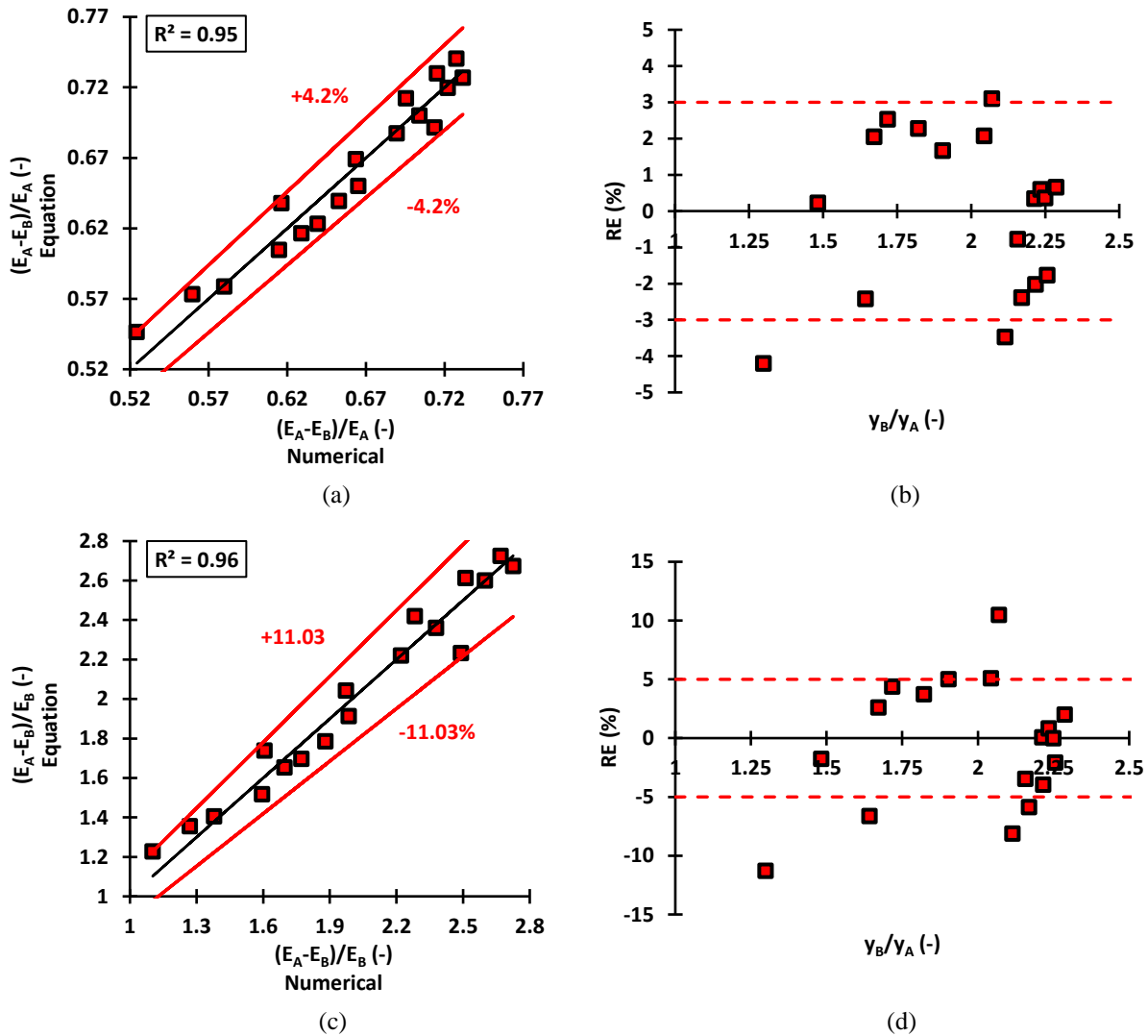

Fig. 7. (a,c) Comparison of calculated and numerical values of relative energy dissipation (b,d) Scatter plot of percentage relative error

Here, the equations were presented for predicting the relative energy dissipation. By determining the corresponding values of y_B/y_A, Fr_A and B/W for all the data related to the contractions of 10 and 15 cm as well as the ratio of the energy dissipation to the upstream and downstream specific energy and combining the data, the predicted equations were calculated according to the following process: First, the non-linear form for the proposed equations was determined as a function of three effective dimensionless parameters y_B/y_A, Fr_A and B/W. The general form of the proposed equations was considered as Equ. (17):

$$\frac{\Delta E_{AB}}{E_A}, \frac{\Delta E_{AB}}{E_B} = a(Fr_A)^b \times (\frac{B}{W})^c \times (\frac{y_B}{y_A})^d \qquad (17)$$

The proposed equations were presented according to Equs. (18) and (19) by using Solver in Excel software.

$$\frac{\Delta E_{AB}}{E_A} = 0.4102\,Fr_A^{0.2815} \times (\frac{B}{W})^{0.049} \times (\frac{y_B}{y_A})^{0.0835} \qquad (18)$$

$$\frac{\Delta E_{AB}}{E_B} = 0.4517\,Fr_A^{1.0193} \times (\frac{B}{W})^{0.0439} \times (\frac{y_B}{y_A})^{-0.2448} \qquad (19)$$

In Figure 7(a,c), the comparison chart of calculated and numerical values of energy dissipation relative to upstream and downstream specific energy is shown. The results indicated that the trend of changes in relative energy dissipation from the simulation is the same as the values obtained from the equations. The R^2 is 0.95 and 0.96 for upstream and downstream, respectively. The percentage relative error against the dimensionless parameter y_B/y_A is shown in Figure 7(b,d). Based on Figure 7(b), more than 83% of the data have an error of less than ±3%. In addition, according to Figure 7(d), more than 66% of the data have an error of less than ±5%. In Table 5, a comparison has been made between the present study and the research of Rajaratnam and Hurting [20] that was conducted with a screen.

Table 5. A comparison between previous study with the present study

Rajaratnam and Hurting [20]		Present study			
		B=10 cm		B=15cm	
Fr_A (-)	$\Delta E_{AB}/E_A$ (-)	Fr_A (-)	$\Delta E_{AB}/E_A$ (-)	Fr_A (-)	$\Delta E_{AB}/E_A$ (-)
4.22	0.504	3.97	0.615 (submerged)	4.25	0.639 (submerged)
4.58	0.581	4.65	0.616	4.84	0.665 (submerged)
5.58	0.659	5.48	0.664	5.81	0.714 (submerged)
6.28	0.721	6.37	0.704	6.36	0.695 (submerged)
7.34	0.791	7.24	0.732	7.22	0.727

4. CONCLUSION

In the present research, the relative energy dissipation of supercritical flow was investigated under free and submerged flow conditions with elliptical-shaped contraction using FLOW-3D. The results were compared with sudden contraction. All simulations have been investigated in a wide range of Froude number in the range of 2.8 to 7.5. A mesh block with dimensions of 0.41 cm was used based on statistical indicators (RE%, AE, RMSE, and KGE). In addition, a comparison of data from numerical solutions with experimental showed that the RNG turbulence model has high accuracy compared to k-ε, k-ω, and LES turbulence models and is in good agreement with experimental data. Based on the results obtained from the simulation, in all cases of using the elliptical-shaped contraction, the energy dissipation is more than the classical free hydraulic jump. The results showed that the Froude number is one of the effective variables in energy dissipation and the energy dissipation increases with increasing it. The results showed that the use of elliptical-shaped contraction has led to a decrease in the Froude number in the range of 1.6 to 2.3 downstream of the contraction. This decrease in the Froude number indicates a decrease in energy. The energy dissipation has increased with the increase in the ratio of the flow depth after the elliptical contraction to the flow depth after the gate. The comparison of the results obtained from the relative energy dissipation in the elliptical-shaped contraction and sudden contraction indicates that the elliptical cross-section performs better than the sudden contraction cross-section. In this study, non-linear polynomial regression equations were presented to estimate the relative energy dissipation,

which are a function of the effective dimensionless parameters y_B/y_A, Fr_A, and B/W. The effect of these parameters caused the accuracy of the equations in this

research improve significantly compared to the previous equations presented by other studies

References

[1] Yarnell, D.L. Bridge piers as channel obstructions. Washington: U.S. Dept. of Agriculture (1934).

[2] Chow, V.R. Open-Channel Hydraulics. New York: McGraw-Hill (1959).

[3] Henderson, F.M. Open channel flow. New York: Macmillan (1966).

[4] Hager, W.H., Dupraz, P.A. Discharge characteristics of local, discontinuous contractions. Journal of Hydraulic Research. 23(5) 421-433 (1985).

[5] Wu, B., Molinas, A. Chocked Flows through Contractions. Journal of Hydraulic Engineering. 127(8) 657-662 (2001).

[6] Dey, S., Raikar, R.V. Scour in Long Contractions. Journal of Hydraulic Engineering, 131(12) 1036-1049 (2005).

[7] Jan, C.D., Chang, C.J. Hydraulic Jumps in an Inclined Rectangular Chute Contraction. Journal of Hydraulic Engineering. 135(11) 949-958 (2009).

[8] Das, R., Pal, D., Das, S., Mazumdar, A. Study of Energy Dissipation on Inclined Rectangular Contracted Chute. Arab J Sci Eng. 39(10) 6995–7002 (2014).

[9] Sadeghfam, S., Akhtari, A.A., Daneshfaraz, R., Tayfur, G. Experimental investigation of screens as energy dissipaters in submerged hydraulic jump. Turkish Journal of Engineering and Environmental Sciences. 38(2) 126-138 (2015).

[10] Babaali, H., Shamsai, A., Vosoughifar, H. Computational Modeling of the Hydraulic Jump in the Stilling Basin with Convergence Walls Using CFD Codes. Arab J Sci Eng. 40(2) 381–395 (2015).

[11] Habibzadeh, A., Rajaratnam, N., Loewen, M. Characteristics of the Flow Field Downstream of Free and Submerged Hydraulic Jumps. Proceedings of the Institution of Civil Engineers-Water Management. 172(4) 180–194 (2019) Doi:10.1680/jwama.17.00004

[12] Ghaderi, A., Dasineh, M., Aristodemo, F., Ghahramanzadeh, A. Characteristics of free and submerged hydraulic jumps over different macroroughnesses. Journal of Hydroinformatics. 22(6) 1554–1572 (2020).

[13] Ghaderi, A. Dasineh, M., Aristodemo, F., Aricò, C. Numerical Simulations of the Flow Field of a Submerged Hydraulic Jump over Triangular Macroroughnesses. Water. 13(5) 674 (2021).

[14] Belaud, G., Cassan, L., Baume, J.P. Calculation of Contraction Coefficient under Sluice Gates and Application to Discharge Measurement. Journal of Hydraulic Engineering. 135(12) 1086-109 (2009).

[15] Daneshfaraz, R., Norouzi, R., Abbaszadeh, H., Azamathulla, H.M. Theoretical and experimental analysis of applicability of sill with different widths on the gate discharge coefficients. Water Supply. 22(10) 7767–7781 (2022) doi: https://doi.org/10.2166/ws.2022.354.

[16] Flow Science Inc. 2016 FLOW-3D V 11.2 User's Manual, Santa Fe, NM, USA; (2016).

[17] Daneshfaraz, R., Norouzi, R., Abbaszadeh, H., Kuriqi, A., Di Francesco, S. Influence of Sill on the Hydraulic Regime in Sluice Gates: An Experimental and Numerical Analysis. Fluids. 7(7) 244 (2022) https://doi.org/10.3390/fluids7070244.

[18] Daneshfaraz, R., Abbaszadeh, H., Gorbanvatan, P., Abdi, M. Application of Sluice Gate in Different Positions and Its Effect on Hydraulic Parameters in Free-Flow Conditions. Journal of Hydraulic Structures. 7(3) 72-87 (2021).

[19] Daneshfaraz, R., Rezazadeh-Joudi., A. and Sadeghfam, S. Experimental Investigation of Energy Dissipation in the Sudden Chocked Flow with free Surfaces. Journal of Civil and Environmental Engineering, 48(2) 101-108 (2018).

[20] Rajaratnam, N., Hurtig, K.I. Screen-type energy dissipator for hydraulic structures. J Hydraul Eng. https://doi.org/10.1061/(ASCE)0733-9429(2000)126:4(310) (2000)